Rem uncouples excitation–contraction coupling in adult skeletal muscle fibers

Donald Beqollari,[1] Christin F. Romberg,[1] Dilyana Filipova,[2] Ulises Meza,[1,3] Symeon Papadopoulos,[2] and Roger A. Bannister[1]

[1]Department of Medicine-Cardiology Division, University of Colorado Denver-Anschutz Medical Campus, Aurora, CO 80045
[2]Institute of Vegetative Physiology, University Hospital of Köln, D-50931 Köln, Germany
[3]Departamento de Fisiología y Biofísica, Facultad de Medicina, Universidad Autónoma de San Luis Potosí, 78210 San Luis Potosí, Mexico

In skeletal muscle, excitation–contraction (EC) coupling requires depolarization-induced conformational rearrangements in L-type Ca^{2+} channel ($Ca_V1.1$) to be communicated to the type 1 ryanodine-sensitive Ca^{2+} release channel (RYR1) of the sarcoplasmic reticulum (SR) via transient protein–protein interactions. Although the molecular mechanism that underlies conformational coupling between $Ca_V1.1$ and RYR1 has been investigated intensely for more than 25 years, the question of whether such signaling occurs via a direct interaction between the principal, voltage-sensing α_{1S} subunit of $Ca_V1.1$ and RYR1 or through an intermediary protein persists. A substantial body of evidence supports the idea that the auxiliary β_{1a} subunit of $Ca_V1.1$ is a conduit for this intermolecular communication. However, a direct role for β_{1a} has been difficult to test because β_{1a} serves two other functions that are prerequisite for conformational coupling between $Ca_V1.1$ and RYR1. Specifically, β_{1a} promotes efficient membrane expression of $Ca_V1.1$ and facilitates the tetradic ultrastructural arrangement of $Ca_V1.1$ channels within plasma membrane–SR junctions. In this paper, we demonstrate that overexpression of the RGK protein Rem, an established β subunit–interacting protein, in adult mouse flexor digitorum brevis fibers markedly reduces voltage-induced myoplasmic Ca^{2+} transients without greatly affecting $Ca_V1.1$ targeting, intramembrane gating charge movement, or releasable SR Ca^{2+} store content. In contrast, a β_{1a}-binding–deficient Rem triple mutant (R200A/L227A/H229A) has little effect on myoplasmic Ca^{2+} release in response to membrane depolarization. Thus, Rem effectively uncouples the voltage sensors of $Ca_V1.1$ from RYR1-mediated SR Ca^{2+} release via its ability to interact with β_{1a}. Our findings reveal Rem-expressing adult muscle as an experimental system that may prove useful in the definition of the precise role of the β_{1a} subunit in skeletal-type EC coupling.

The Journal of General Physiology

INTRODUCTION

Excitation–contraction (EC) coupling is the physiological event in which muscle converts an electrical signal (plasma membrane depolarization) into mechanical work (muscle contraction). In the case of skeletal muscle, depolarization-induced conformational rearrangements within the L-type Ca^{2+} channel complex ($Ca_V1.1$) are coupled to gating of the type 1 ryanodine-sensitive Ca^{2+} release channel (RYR1) of the SR (Schneider and Chandler, 1973; Ríos and Brum, 1987; Tanabe et al., 1988). The resultant Ca^{2+} efflux from the SR into the myoplasm via RYR1 activates the contractile filaments. Because SR Ca^{2+} release occurs rapidly in response to depolarization and independently of transient Ca^{2+} fluctuations, a conformational coupling mechanism appears to support communication between the two channels (see Bannister and Beam, 2013).

Although the roles of $Ca_V1.1$ and RYR1 as voltage sensor and SR Ca^{2+} release channel, respectively, have been established for quite some time (Tanabe et al., 1988; Nakai et al., 1996), the molecular mechanics that support conformational coupling between these two channels remain undefined. One candidate structure to mediate such coupling is the intracellular segment that links repeats II and III of the principal α_{1S} subunit of $Ca_V1.1$ (Tanabe et al., 1990; Lu et al., 1994; Nakai et al., 1998; Wilkens et al., 2001). Another viable candidate is the auxiliary β_{1a} subunit of the $Ca_V1.1$ heteromultimer. In this regard, β_{1a} is firmly established as being essential for EC coupling, as genetic deletion of β_1 abolishes voltage-dependent SR Ca^{2+} release in both mammals and bony fish (Gregg et al., 1996; Ono et al., 2004; Schredelseker et al., 2005, 2009). Moreover, purified β_{1a} subunits and β_{1a} peptide fragments bind RYR1 in vitro and/or activate RYR1 in planar lipid bilayers (Cheng et al., 2005; Rebbeck et al., 2011; Karunasekara et al., 2012; Hernández-Ochoa et al., 2014). Still, the key roles of β_{1a} in trafficking

Correspondence to Roger A. Bannister: roger.bannnister@ucdenver.edu

Abbreviations used in this paper: 4-C*m*C, 4-chloro-*m*-cresol; CRU, Ca^{2+} release unit; EC, excitation–contraction; FDB, flexor digitorum brevis; RYR1, type 1 ryanodine-sensitive Ca^{2+} release channel.

The Rockefeller University Press $30.00
J. Gen. Physiol. Vol. 146 No. 1 97–108
www.jgp.org/cgi/doi/10.1085/jgp.201411314

$Ca_V1.1$ to the plasma membrane (Gregg et al., 1996; Strube et al., 1996) and in the ultrastructural organization of $Ca_V1.1$ into the tetradic arrays prerequisite for EC coupling (Schredelseker et al., 2005, 2009; Dayal et al., 2010, 2013; Eltit et al., 2014) have made testing a direct role for β_{1a} in communication between the voltage-sensing components of $Ca_V1.1$ and RYR1-mediated SR Ca^{2+} release highly problematic.

Members of the RGK (Rad, Rem, Rem2, Gem/Kir) family of monomeric G proteins inhibit L-type Ca^{2+} channels in a variety of physiological systems via interactions that occur primarily with the β subunit (Béguin et al., 2001, 2007; Finlin et al., 2003, 2006; Murata et al., 2004; Bannister et al., 2008; Yang et al., 2012; Romberg et al., 2014; Xu et al., 2015; reviewed recently by Yang and Colecraft, 2013). In the present study, we have examined the impact of Rem on EC coupling in adult mouse flexor digitorum brevis (FDB) fibers overexpressing Rem via in vivo electroporation (DiFranco et al., 2007). Using this approach, we have found that Rem effectively uncouples the $Ca_V1.1$ voltage sensor from RYR1-mediated SR Ca^{2+} release through its interaction with β_{1a}. Specifically, Rem markedly reduces voltage-induced myoplasmic Ca^{2+} transients without appreciable effects on $Ca_V1.1$ targeting, intramembrane charge movement, or SR Ca^{2+} store content.

MATERIALS AND METHODS

Molecular biology

CFP-$Ca_V1.1$. A cDNA encoding a CFP-rabbit $Ca_V1.1$ α_{1S}-subunit (GenBank accession no. X05921) fusion construct was created by swapping out YFP for CFP in an existing YFP–α_{1S} fusion construct (Papadopoulos et al., 2004). The cDNA segment encoding CFP was excised from the parent pECFP-C1 vector (Takara Bio Inc.) using NheI and HindIII (761 bp). Likewise, YFP was removed from the YFP–α_{1S} fusion construct using the same restriction enzymes, linearizing the pEYFP-C1 backbone and the α_{1S}-coding sequence (9,555 bp). The CFP-encoding segment was then religated into the linearized vector carrying the α_{1S}-coding sequence (final, 10,316 bp).

CFP-β_{1a} and YFP-β_{1a}. The constructions of CFP–rabbit β_{1a} and YFP–rabbit β_{1a} (both GenBank accession no. M25514) were described previously by Leuranguer et al. (2006); CFP-β_{1a}, YFP-β_{1a}, and CFP-$Ca_V1.1$ were all provided by K.G. Beam (University of Colorado Denver-Anschutz Medical Campus, Aurora, CO).

V-Rem AAA. The construction of V-Rem AAA (RefSeq accession no. NP_033073) was described previously by Beqollari et al. (2015). Restriction digests and sequencing were used to verify all constructs.

In vivo electroporation and dissociation of FDB fibers

All procedures involving mice were approved by the University of Colorado Denver-Anschutz Medical Campus Institutional Animal Care and Use Committee. cDNA plasmids encoding YFP, CFP-α_{1S}, CFP-β_{1a}, V-Rem, and/or V-Rem AAA were delivered to FDB fibers of anesthetized 2–3-mo-old male C57BL/6J mice (The Jackson Laboratory) via an in vivo electroporation protocol similar to that originally described by DiFranco et al. (2007). In brief, 10 µl of 2 mg/ml hyaluronidase solution was injected into the FDB muscle with a 30-gauge hypodermic needle. After 1 h, mice were re-anesthetized and 20 µl cDNA (3–5 µg/µl) was injected into the muscle. 5 min later, two gold-plated acupuncture needle electrodes (Lhasa OMS) coupled to an isolated pulse stimulator (A-M Systems) were placed subcutaneously near the proximal and distal tendons of the muscle (∼1 cm apart). cDNAs were then electroporated into the FDB muscle with 20 100-V, 20-ms pulses delivered at 1 Hz. For assessment of SR Ca^{2+} stores, the transfection mixture also contained 5 µg pmCherry-C1 (Takara Bio Inc.) as a means to identify successfully transfected fibers after loading with Fluo 3-AM dye (Invitrogen; see below).

Electroporated (9–10 d after transfection) FDB muscles were dissected in cold rodent Ringer's solution (mM: 146 NaCl, 5 KCl, 2 $CaCl_2$, 1 $MgCl_2$, and 10 HEPES, pH 7.4 with NaOH). Muscles were then digested in a collagenase solution (mM: 155 Cs-aspartate, 10 HEPES, and 5 $MgCl_2$, pH 7.4 with CsOH, supplemented with 1 mg/ml BSA [Sigma-Aldrich] and 1 mg/ml collagenase type IA [Sigma-Aldrich]) with agitation at 37°C for ∼1 h. Immediately after digestion, the collagenase solution was replaced with a dissociation solution (mM: 140 Cs-aspartate, 10 Cs_2EGTA, 10 HEPES, and 5 $MgCl_2$, pH 7.4 with CsOH, supplemented with 1 mg/ml BSA), and muscles were triturated gently with a series of fire-polished glass pipettes of descending bore. Dissociated FDB fibers destined for whole-cell patch-clamp experiments were then plated onto ECL (EMD Millipore)-coated 35-mm plastic culture dishes (Falcon). For imaging, fibers were allowed to settle onto laminin (Invitrogen)-coated 35-mm culture dishes with glass coverslip bottoms (MatTek). Experiments were performed with FDB fibers 1–6 h after dissociation; successfully transfected fibers were identified by the presence of YFP or Venus fluorescence.

Measurement of intramembrane charge movements and L-type Ca^{2+} currents from FDB fibers

Patch pipettes were fabricated from borosilicate glass and had resistances of ≤1.0 MΩ when filled with internal solution, which consisted of (mM): 140 Cs-aspartate, 10 Cs_2-EGTA, 5 $MgCl_2$, and 10 HEPES, pH 7.4 with CsOH; fibers were dialyzed in the whole-cell configuration for >20 min before recording. For recording of L-type Ca^{2+} currents, the external solution contained (mM): 145 TEA-methanesulfonic acid, 10 $CaCl_2$, 10 HEPES, 2 $MgSO_4$, 1 4-aminopyridine, 0.1 anthracene-9-carboxylic acid, and 0.002 tetrodotoxin, pH 7.4 with TEA-OH. For measurement of charge movements, the bath contained (mM): 145 TEA-methanesulfonic acid, 10 $CaCl_2$, 10 HEPES, 2 $MgSO_4$, 1 4-aminopyridine, 0.1 anthracene-9-carboxylic acid, 0.002 tetrodotoxin, 1 $LaCl_3$, and 0.5 $CdCl_2$, pH 7.4 with TEA-OH. Linear components of leak and capacitive current were corrected with −P/4 online subtraction protocols. Output filtering was at 2–5 kHz, and digitization was either at 5 kHz (currents) or 10 kHz (charge movements). Cell capacitance was determined by integration of a transient from −80 to −70 mV using Clampex 10.3 (Molecular Devices) and was used to normalize charge movement (nC/µF) and current amplitude (pA/pF). The average value of C_m was 2.3 ± 0.1 nF (n = 48 fibers). To minimize voltage error, the time constant for decay of the whole-cell capacity transient (τ_m) was reduced as much as possible using the analogue compensation circuit of the amplifier; the average values of τ_m and R_a were 1.0 ± 0.02 ms and 467 ± 26 kΩ, respectively. Q_{ON} was then normalized to C_m and plotted as a function of test potential (V), and the resultant Q-V relationship was fitted according to:

$$Q_{ON} = Q_{max} \Big/ \left\{1 + \exp\left[\left(V_Q - V\right)/k_Q\right]\right\}, \quad (1)$$

where Q_{max} is the maximal Q_{ON}, V_Q is the potential causing movement of half the maximal charge, and k_Q is a slope parameter.

Peak currents were normalized to C_m, and the resultant I-V was fitted according to:

$$I = G_{max} * (V - V_{rev}) / \{1 + \exp[-(V - V_{1/2})/k_G]\}, \quad (2)$$

where I is the normalized current for the test potential V, V_{rev} is the reversal potential, G_{max} is the maximum Ca^{2+} channel conductance, $V_{1/2}$ is the half-maximal activation potential, and k_G is the slope factor. All electrophysiological and Ca^{2+}-imaging experiments were performed at room temperature (~25°C).

Measurement of intracellular Ca^{2+} transients in the whole-cell configuration

Voltage-induced changes in myoplasmic Ca^{2+} were recorded from FDB fibers with Fluo 3 single-wavelength Ca^{2+} indicator dye (Invitrogen). The pentapotassium salt form of the dye was added to the standard internal solution (see above) for a final concentration of 200 µM. The external solution contained (mM): 145 TEA-methanesulfonic acid, 10 $CaCl_2$, 10 HEPES, 2 $MgSO_4$, 1 4-aminopyridine, 0.1 anthracene-9-carboxylic acid, and 0.002 tetrodotoxin, pH 7.4 with TEA-OH. After entry into the whole-cell configuration, a waiting period of no less than 20 min was used to allow the dye to diffuse into the cell interior. A 100-W mercury illuminator and a set of fluorescein filters were used to excite the dye present in the voltage-clamped fiber. A computer-controlled shutter was used to block illumination in the intervals between test pulses. Fluorescence emission was measured by means of a fluorometer (Biomedical Instrumentation Group, University of Pennsylvania). Fluorescence data are expressed as ΔF/F, where ΔF represents the change in peak fluorescence from baseline during the test pulse, and F is the fluorescence immediately before the test pulse minus the average background fluorescence. The peak value of the fluorescence change (ΔF/F) for each test potential (V) was fitted according to:

$$(\Delta F/F) = (\Delta F/F)_{max} / \{1 + \exp[(V - V_F)/k_F]\}, \quad (3)$$

where $(\Delta F/F)_{max}$ is the maximal fluorescence change, V_F is the potential causing half the maximal change in fluorescence, and k_F is a slope parameter. Only cells with transients that could be fit with Eq. 3 were used for analysis.

Live cell imaging

Dissociated FDB fibers were examined in rodent Ringer's solution using a confocal laser-scanning microscope (LSM 510 META; Carl Zeiss). A Plan-Apochromat 63× oil-immersion objective (1.4 NA) was used to view the fiber of interest. CFP and Venus were excited with separate sweeps of the 458- and 514-nm lines, respectively, of an argon laser (30-milliwatt maximum output, operated at 50% or 6.3 A) directed to the cell via a 458/514-nm dual dichroic mirror. The emitted fluorescence was split via a 515-nm long-pass filter; CFP was directed to a photomultiplier equipped with a 465–495-nm band-pass filter, and Venus was directed to a photomultiplier equipped with a 530-nm long-pass filter. The chosen settings precluded recording of fluorescence bleed between CFP and Venus, because CFP is not excited at 514 nm and Venus emission is negligible between 465 and 495 nm (see Papadopoulos et al., 2004). Confocal fluorescence intensity data were recorded as the average of eight line scans per pixel and digitized at 8 bits, with photomultiplier gain adjusted such that maximum pixel intensities were no more than ~70% saturated.

Assessment of SR Ca^{2+} store content

FDB fibers were loaded with 5 µM Fluo 3-AM and 0.05% pluronic acid (both from Invitrogen) dissolved in rodent Ringer's solution for 35 min at 37°C. Fibers were then washed three times in rodent Ringer's solution with gentle agitation. After a 10-min de-esterification period, Fluo 3-AM–loaded cells bathed in rodent Ringer's solution were placed on the stage of the LSM 510 META microscope and viewed with a 10× 0.3-NA objective (Carl Zeiss). Fluo 3-AM was excited with the 488-nm line of an argon laser (30-milliwatt maximum output, operated at 50% or 6.3 A, attenuated to 5%). The emitted fluorescence was directed through a dual 488/543 dichroic mirror to a photomultiplier equipped with a 500–530-nm band-pass filter. SR Ca^{2+} release was induced by 1 mM 4-chloro-*m*-cresol (4-C*m*C; Pfaltz & Bauer) delivered via a manually operated, gravity-driven global perfusion system. Fluorescence amplitude data are expressed as ΔF/F, where F represents the baseline fluorescence before application of 4-C*m*C, and ΔF represents the change in peak fluorescence during the application of 4-C*m*C.

tsA201 cell culture and expression of cDNA

Low (<20) passage tsA201 cells were propagated in culture medium containing 90% DMEM (Thermo Fisher Scientific), 10% defined fetal bovine serum (GE Healthcare), and 100 µg/ml penicillin-streptomycin (Life Technologies). Cells were trypsinized twice weekly and replated onto 35-mm culture dishes at ~20% confluence. Lipofectamine 2000 (Life Technologies) was used to transfect these cells within 3–5 d of plating. The transfection mixture contained expression plasmids encoding rat $Ca_V1.3$, rabbit β_{1a}, and rat $\alpha_2\delta1$ channel subunits at 1 µg of each cDNA per dish. The transfection mixture also contained a plasmid-encoding Venus–Rem construct (1 µg/dish; see above) or YFP (30 ng/dish; Takara Bio Inc.). The day after transfection, cells were trypsinized and replated onto 35-mm plastic for experiments the next day.

Coimmunoprecipitation

tsA201 cells expressing YFP-β_{1a}, YFP-β_{1a}/V-Rem, or YFP-β_{1a}/V-Rem AAA were lysed into 300 µl of lysis buffer (mM: 50 Tris-HCl, pH 7.5, 100 NaCl, 1 $MgCl_2$, 1 DTT, and 0.2% Tween-20) supplemented with 0.1 mM iodoacetamide and 1 mM phenylmethylsulfonyl fluoride (both from Thermo Fisher Scientific). After insoluble material was removed by centrifugation, the homogenates were incubated with a monoclonal antibody directed to Rem (1:200; Santa Cruz Biotechnology, Inc.) for 4–6 h with gentle agitation followed by an overnight incubation with protein A agarose beads (Santa Cruz Biotechnology, Inc.). The agarose beads were then washed twice with lysis buffer and collected after gentle centrifugation at 2,500 rpm. The beads were then resuspended in 30 µl of 1% SDS buffer (Bio-Rad Laboratories) and subjected to SDS-PAGE analysis. Proteins were transferred into a nitrocellulose membrane, blocked with 3% nonfat dry milk (Kroger) in PBS-Tween, and incubated overnight at 4°C with monoclonal antibodies directed to either X(G)FP (1:1,500; Antibodies Inc.) or Rem (1:500). The nitrocellulose membrane was then washed three times with PBS-Tween and incubated at room temperature for 1 h with horseradish peroxidase–conjugated goat anti–mouse IgG (1:10,000; SouthernBiotech). Protein bands were visualized with the SuperSignal West Femto kit (Thermo Fisher Scientific) and viewed on a FluorChem HD2 scanner (Alpha Innotech). Blots were stripped using Restore Western Blot Stripping Buffer (Thermo Fisher Scientific).

L-type Ca^{2+} current recordings from tsA201 cells

Borosilicate pipettes (2.0–3.0 MΩ) were filled with internal solution, which consisted of (mM): 140 Cs-aspartate, 10 Cs_2-EGTA, 5 $MgCl_2$, and 10 HEPES, pH 7.4 with CsOH. The bath solution contained (mM): 145 NaCl, 10 $CaCl_2$, and 10 HEPES, pH 7.4 with NaOH. Electronic compensation was used to reduce the effective series resistance, and linear components of leak and capacitive current were corrected with −P/4 online subtraction protocol. Filtering and digitation were at 2 and 5 kHz, respectively. For tsA201 cell experiments, the average values of C_m, τ_m, and R_a were 20.0 ± 1.4 pF, 202.0 ± 18.9 µs, and 10.9 ± 0.9 MΩ, respectively (n = 28 cells).

Analysis

All data are presented as mean ± SEM. Statistical comparisons were made by unpaired *t* test or by one-way ANOVA (where appropriate), with $P < 0.05$ considered significant. Figures were made using the software program SigmaPlot (version 11.0; SSPS Inc.).

Online supplemental material

Fig. S1 shows, qualitatively, the successful expression of both V-Rem and V-Rem AAA in FDB fibers by in vivo electroporation. Confocal fluorescence images of six different live, intact FDB fibers overexpressing V-Rem or V-Rem AAA are shown with average intensity profiles for the indicated regions of interest. Online supplemental material is available at http://www.jgp.org/cgi/content/full/jgp.201411314/DC1.

RESULTS

Rem inhibits EC coupling in FDB fibers without affecting intramembrane charge movement

Recently, we described the effects of the RGK proteins Rad and Rem on L-type Ca^{2+} currents and intramembrane charge movement in adult FDB muscle fibers (Beqollari et al., 2014). Although both Rad and Rem inhibited L-type currents by ∼60 and ∼45%, respectively, charge movement was only reduced in fibers transfected with Rad; charge movement for Rem-expressing fibers was virtually identical to charge movement observed in naive fibers. To confirm the latter observation, we used in vivo electroporation (DiFranco et al., 2007) to transfect FDB muscles of otherwise normal 2–3-mo-old C57BL/6J mice with either YFP or a Venus-fused wild-type mouse Rem construct (V-Rem). As expected, FDB fibers overexpressing V-Rem again displayed maximal charge movement virtually identical to YFP-expressing fibers in both amplitude and voltage dependence (Fig. 1, A–C and Table 1). Both Q-V relationships were similar to that reported by Prosser et al. (2009) when La^{3+} was included in the extracellular recording solution.

Because skeletal muscle EC coupling is coupled directly to translocation of $Ca_V1.1$'s voltage-sensing structures (Schneider and Chandler, 1973; Ríos and Brum, 1987; García et al., 1994; Tanabe et al., 1988), we next investigated the impact of Rem on EC coupling by recording myoplasmic Ca^{2+} transients in response to membrane depolarization (as in Wang et al., 1999; Wu et al., 2012). Ca^{2+} transients recorded from fibers transfected with V-Rem were substantially reduced compared with the transients of YFP-expressing fibers (0.6 ± 0.1 ΔF/F, $n = 8$ vs. 1.6 ± 0.4 ΔF/F, $n = 6$, respectively; $P < 0.001$; Fig. 1, D–F). No significant effect on the voltage dependence of SR Ca^{2+} release was observed between the two groups ($P > 0.05$; Table 1).

SR Ca^{2+} store content is not significantly affected by overexpression of Rem

As a means to determine whether the V-Rem–mediated reduction in voltage-induced Ca^{2+} release was a consequence

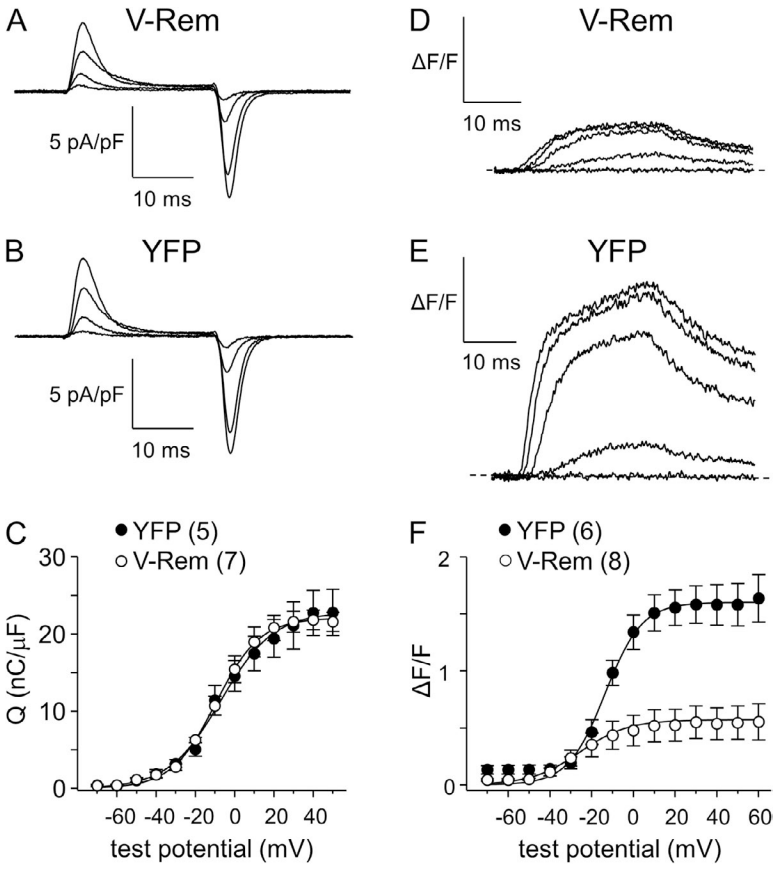

Figure 1. Rem inhibits EC coupling in FDB fibers without affecting intramembrane charge movement. Representative recordings of intramembrane charge movements elicited by 25-ms depolarizations from −80 to −40, −20, 0, and 20 mV shown for transfected FDB fibers expressing either V-Rem (A) or YFP (B). (C) The Q-V relationships for fibers expressing either V-Rem ($n = 7$; ○) or YFP ($n = 5$; ●) are shown. Charge movements were evoked at 0.1 Hz by test potentials ranging from −70 through 50 mV in 10-mV increments. The smooth curves for V-Rem– or YFP-expressing fibers are plotted according to Eq. 1, with the respective fit parameters shown in Table 1. Representative recordings of myoplasmic Ca^{2+} transients elicited by 25-ms depolarizations from −80 to −40, −20, 0, 20, and 40 mV are shown for FDB fibers overexpressing V-Rem (D) or YFP (E). (F) The peak ΔF/F-V relationships for V-Rem ($n = 8$; ○)– and YFP ($n = 6$; ●)-expressing fibers are shown. Ca^{2+} transients were evoked at 0.1 Hz by test potentials ranging from −70 through 60 mV in 10-mV increments. The smooth curves for V-Rem– and YFP-expressing fibers are plotted according to Eq. 3 with the respective fit parameters shown in Table 1. Error bars represent ±SEM.

TABLE 1

Charge movement and Ca^{2+} release fit parameters

Construct	Q-V			ΔF/F-V		
	Q_{max}	V_Q	k_Q	$\Delta F/F_{max}$	V_F	k_F
	nC/μF	*mV*	*mV*	*ΔF/F*	*mV*	*mV*
YFP	22.8 ± 3.4 (5)	−7.8 ± 3.5	12.0 ± 1.7	1.6 ± 0.2 (6)	−13.0 ± 1.2	8.4 ± 0.8
V-Rem	22.4 ± 1.2 (7)	−8.1 ± 1.6	11.8 ± 1.6	0.6 ± 0.1[a] (8)	−20.2 ± 4.7	14.7 ± 2.6
V-Rem AAA	24.6 ± 3.4 (5)	−8.5 ± 1.0	8.1 ± 1.0	1.4 ± 0.2 (6)	−15.5 ± 1.3	9.9 ± 0.9

Data are given as mean ± SEM, with the numbers in parentheses indicating the number of FDB fibers tested. Charge movement and EC coupling data were fit by Eqs. 1 and 3, respectively. Only cells with Ca^{2+} transients that could be fit with Eq. 3 were used for analysis; two Rem-expressing fibers lacking quantifiable ΔF/F were dropped. One significant difference between the three groups is indicated.
[a]$P < 0.001$; one-way ANOVA.

of an altered SR Ca^{2+} store, we exposed intact fibers loaded with Fluo-3 AM dye to the RYR agonist 4-C*m*C. In these experiments, 1 mM 4-C*m*C elicited SR Ca^{2+} release that was nearly indistinguishable between FDB fibers overexpressing V-Rem and fibers expressing YFP only (5.7 ± 1.0 ΔF/F, $n = 9$ vs. 6.8 ± 1.8 ΔF/F, $n = 5$, respectively; $P > 0.05$; Fig. 2, A–C). The equivalent responses of YFP- and V-Rem–expressing fibers to 4-C*m*C suggest that depletion of SR Ca^{2+} store is an unlikely explanation for the ∼65% reduction in Ca^{2+} transient amplitude observed in V-Rem–expressing fibers.

Rem overexpression does not alter targeting of $Ca_V1.1$ α_{1S} or β_{1a} subunits

Because Rem has been reported to alter high voltage-activated Ca^{2+} channel trafficking in heterologous systems (Béguin et al., 2007; Mahalakshmi et al., 2007; Flynn and Zamponi, 2010; Yang et al., 2010) and in cardiac myocytes (Jhun et al., 2012), one possible explanation for the disruption of EC coupling by V-Rem (Fig. 1, D and F) is that the small G protein redirects $Ca_V1.1$ away from triad junctions. For this reason, we examined the subcellular distribution of $Ca_V1.1$ α_{1S} and β_{1a} subunits in the absence and presence of coexpressed V-Rem. When expressed in FDB fibers, CFP-tagged α_{1S} subunits of $Ca_V1.1$ were targeted to transverse tubules as shown previously for YFP-tagged α_{1S} subunits (DiFranco et al., 2011; Fig. 3 A). The tubular distribution of CFP-α_{1S} was unaffected by coexpression of V-Rem (Fig. 3 B). Likewise, coexpression of V-Rem had little, if any, effect on the subcellular distribution of CFP-β_{1a} (Fig. 3, C and D). Interestingly, the V-Rem fluorescence extended from the transverse tubules into the region of the I band. In this regard, the subcellular distribution of V-Rem overlapped, but did not completely match, the transverse tubular distributions of $Ca_V1.1$ α_{1S} and β_{1a} subunits. We do not consider the presence of Rem in the I band to be an artifact of overexpression, as the related RGK protein Rad clearly targets to transverse tubules when expressed in FDB fibers via electroporation (see Beqollari et al., 2014). Moreover, this observation does not affect our interpretation of the data shown in Fig. 3: coexpression

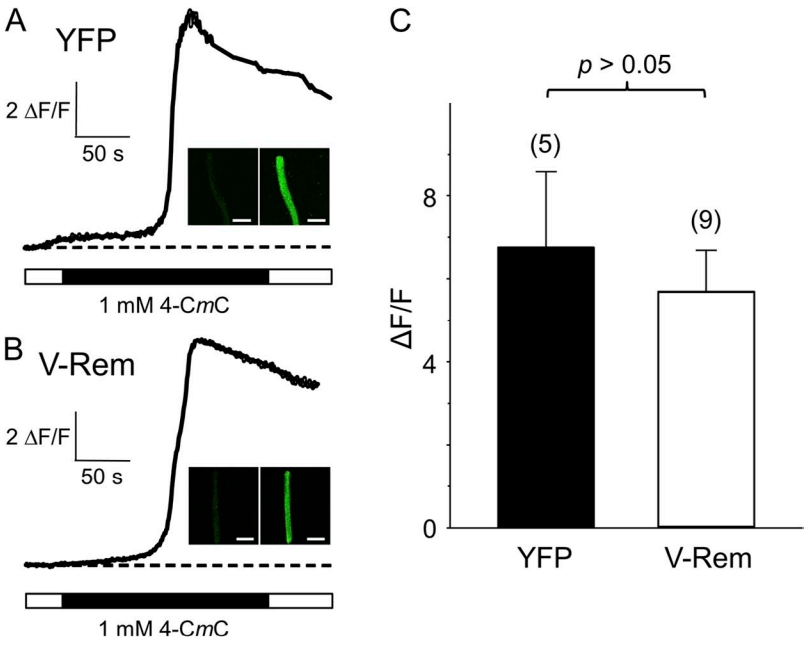

Figure 2. SR Ca^{2+} store content is not significantly affected by overexpression of Rem. SR Ca^{2+} store content as assessed by changes in Fluo-3 AM fluorescence (ΔF/F) in response to the application of 1 mM 4-C*m*C to fibers expressing either YFP (A) or V-Rem (B). Insets show images of loaded fibers before 4-C*m*C application (left) and at the peak of fluorescence (right). Bars, 100 μm. (C) A comparison of the average peak ΔF/F values for YFP- and V-Rem–expressing fibers is shown. Error bars represent ±SEM.

of V-Rem did not alter targeting of the channel subunits to the transverse tubules.

Simultaneous introduction of alanines at Rem positions R200, L227, and H229 disrupts interactions with β_{1a}

So far, our data indicate that Rem uncouples the $Ca_V1.1$ voltage sensor from RYR1-mediated SR Ca^{2+} release. However, it is unclear whether this effect of Rem is dependent on the ability of the small GTP-binding protein to interact with the β_{1a} subunit of the $Ca_V1.1$ channel complex. In this regard, three highly conserved residues of Rem (R200, L227, or H229) have been identified as being critical for interactions with the β_3-subunit isoform (Béguin et al., 2007; Puhl et al., 2014); conversion of any one of these residues to alanine severely impairs binding to β_3-subunit isoforms in both yeast-2-hybrid and coimmunoprecipitation assays. To specifically test whether Rem binds to the β_{1a}-subunit isoform, we engineered a V-Rem–based construct with alanines introduced at positions R200, L227, and H229 (V-Rem AAA) and compared its ability to coimmunoprecipitate with a YFP-fused β_{1a} construct (YFP-β_{1a}). In these experiments, a commercially available monoclonal Rem antibody failed to immunoprecipitate YFP-β_{1a} in lysates obtained from tsA201 cells transfected with only YFP-β_{1a} (shown in duplicate in Fig. 4 A, lanes 2 and 6). In contrast, the antibody efficiently immunoprecipitated YFP-β_{1a} subunits when V-Rem was coexpressed with YFP-β_{1a} (Fig. 4 A, lanes 3 and 7). Consistent with the earlier report of Béguin et al. (2007) showing the disruption of the Rem-β_3 interaction with alanine single-point mutants, an interaction between V-Rem AAA and β_{1a} was not detectable (Fig. 4 A, lanes 4 and 8). In control experiments, the Rem antibody detected similar levels of immunoprecipitated V-Rem and V-Rem AAA (Fig. 4 B, lanes 3–4 and 7–8). Comparable expression levels for YFP-β_{1a}, V-Rem, and V-Rem AAA mutant were confirmed in a Western blot from total lysates collected before coimmunoprecipitation (Fig. 4 C).

V-Rem AAA fails to inhibit L-type channels expressed in tsA201 cells

We next determined the functional consequences of the disruption of the Rem-β_{1a} interaction. In these experiments, we coexpressed YFP, V-Rem, or V-Rem AAA with $Ca_V1.3$ α_{1D}, β_{1a}, and $\alpha_2\delta$-1 subunits to detect interactions that occur within a functional L-type channel complex (we used $Ca_V1.3$ as a surrogate for $Ca_V1.1$ because of its highly efficient and consistent membrane expression in tsA201 cells; see Meza et al., 2013). Predictably, tsA201 cells expressing $Ca_V1.3$, β_{1a}, $\alpha_2\delta$-1, and V-Rem displayed virtually no L-type current (-3.8 ± 0.7 pA/pF

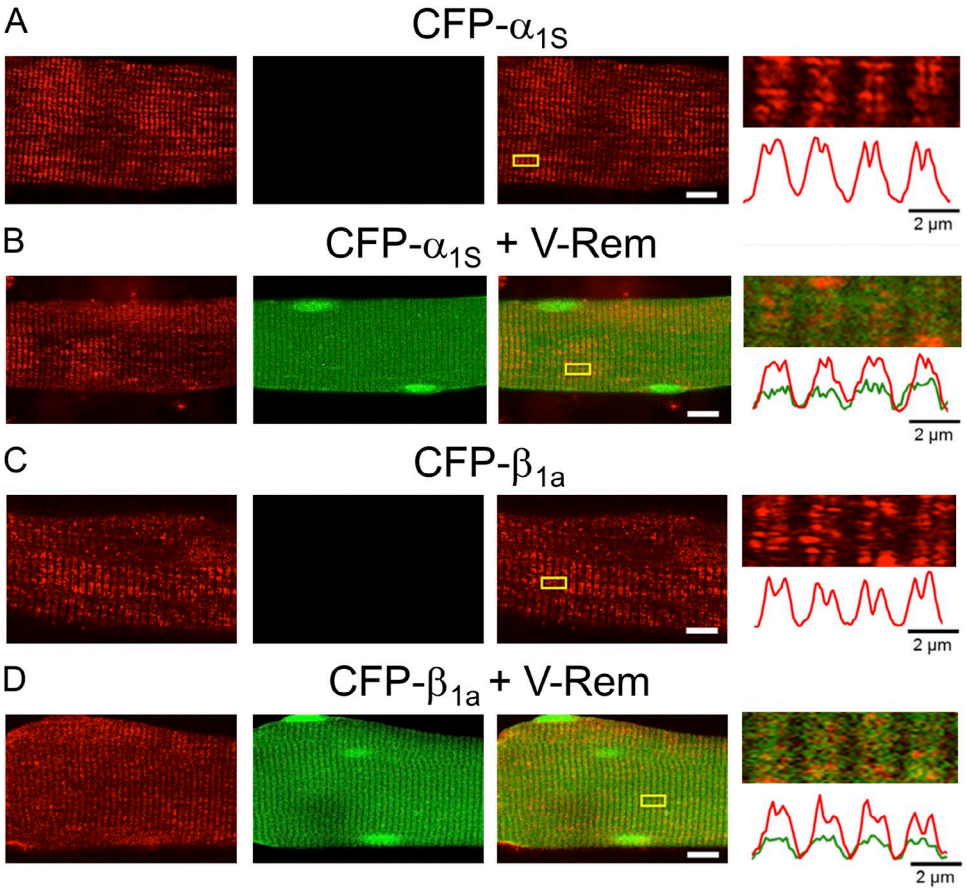

Figure 3. Rem overexpression does not alter targeting of $Ca_V1.1$ α_{1S} or β_{1a} subunits. Confocal images of FDB fibers expressing CFP-α_{1S} alone (A), CFP-α_{1S} coexpressed with V-Rem (B), CFP-β_{1a} alone (C), or CFP-β_{1a} coexpressed with V-Rem (D). For each panel, the left, left-middle, and right-middle images show CFP fluorescence (red), Venus fluorescence (green), and an overlay, respectively. Bars, 10 µm. The right images are blowups of the area indicated by the yellow boxes in the adjacent overlays; average image profile analyses are shown below. The green lines indicate Venus fluorescence and the red lines represent the fluorescence emitted by either CFP-α_{1S} or CFP-β_{1a} in arbitrary units. Note that the transverse-tubular targeting of CFP-α_{1S} or β_{1a} is intact both in the absence and in the presence of coexpressed V-Rem. For experiments with each channel subunit clone, images were acquired with nearly identical microscope settings.

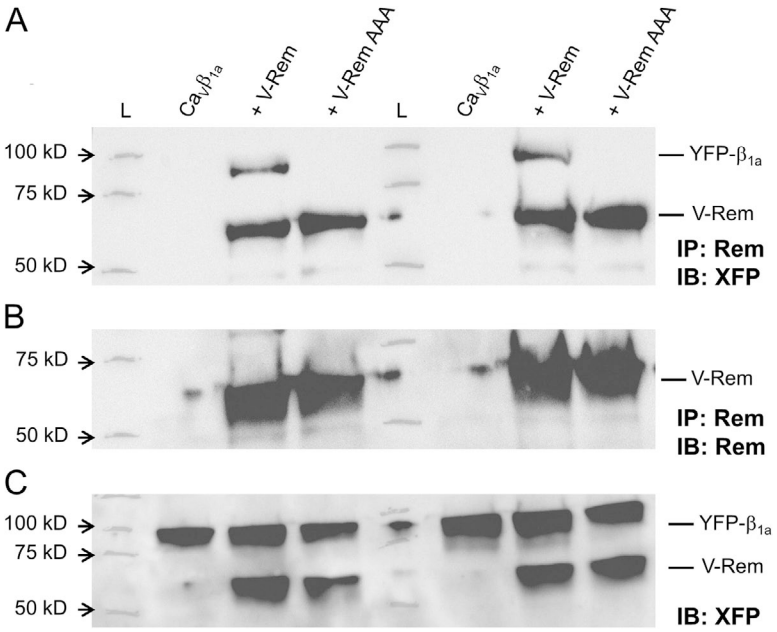

Figure 4. Introduction of alanines at Rem positions R200, L227, and H229 disrupts the interaction with β_{1a}. (A) In the duplicate representative experiments shown, a monoclonal antibody directed to Rem was used to immunoprecipitate V-Rem–YFP-β_{1a} complexes from tsA201 cells expressing YFP-β_{1a} (lanes 2 and 6), YFP-β_{1a} and V-Rem (lanes 3 and 7), and YFP-β_{1a} and V-Rem AAA (lanes 4 and 8). Blots were probed with an antibody directed to XFP (see Materials and methods). (B) Similar affinity of the Rem antibody for V-Rem and V-Rem AAA is presented, where the immunoprecipitated Rem and Rem AAA are detected by the Rem antibody (lanes 3–4 and 7–8). (C) Comparable expression of YFP-β_{1a}, V-Rem, and V-Rem AAA in harvested tsA201 cells is confirmed in total lysates before coimmunoprecipitation. Lanes 1 and 5 are loaded with protein markers (molecular weights indicated). Results shown are representative of five separate experiments.

at 0 mV; $n = 4$; Fig. 5 A). In contrast, cells expressing $Ca_V1.3$, β_{1a}, $\alpha_2\delta$-1, and V-Rem AAA had L-type currents nearly identical in amplitude (-78.3 ± 16.0 pA/pF, $n = 15$; Fig. 5, B and D) to control cells expressing the same channel subunits with a YFP transfection marker (-71.0 ± 20.0 pA/pF, $n = 9$; $P > 0.05$; Fig. 5, C and D). Successful expression of V-Rem and V-Rem AAA in tsA201 cells was indicated by Venus fluorescence (Fig. 5 E).

V-Rem AAA fails to inhibit $Ca_V1.1$ function in FDB fibers

To establish β_{1a} as the mechanistic target of Rem in our experimental system, we overexpressed V-Rem AAA in FDB fibers and assayed its effects on L-type Ca^{2+} currents, intramembrane charge movement, and EC coupling. Successful expression of V-Rem AAA in FDB fibers was confirmed by Venus fluorescence, which was comparable to the fluorescence generated by V-Rem

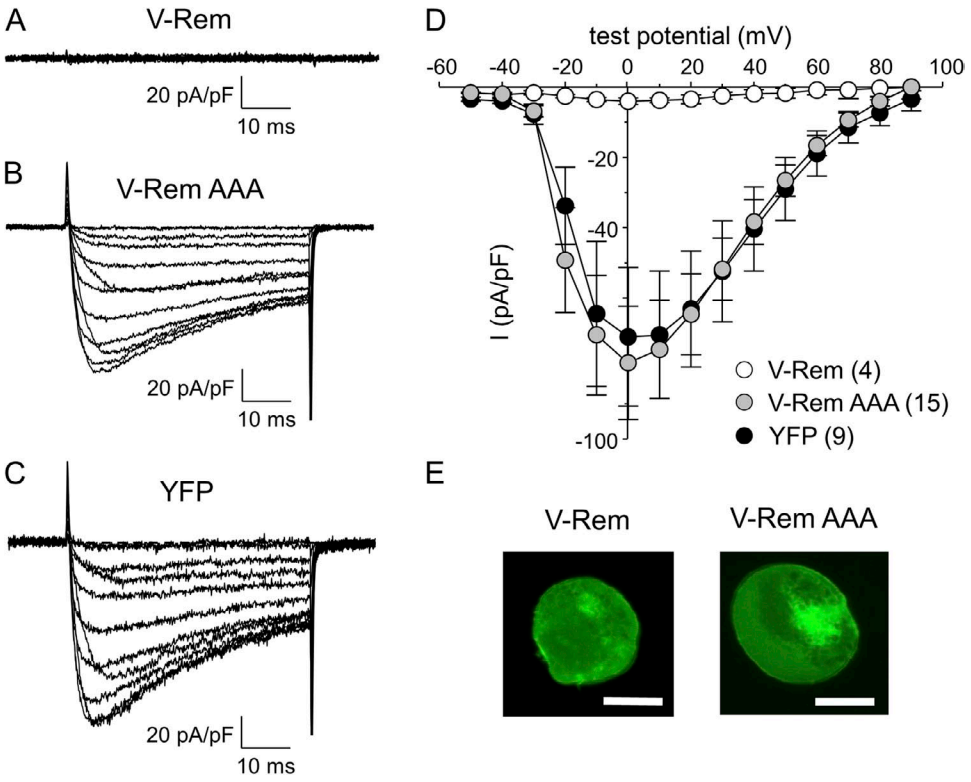

Figure 5. Introduction of alanines at Rem positions R200, L227, and H229 ablates the ability of V-Rem to inhibit L-type Ca^{2+} current conducted by $Ca_V1.3/\beta_{1a}/\alpha_2\delta$-1 channels expressed in tsA201 cells. Representative L-type currents are shown for tsA201 cells coexpressing $Ca_V1.3/\beta_{1a}/\alpha_2\delta$-1 and V-Rem (A), V-Rem AAA (B), or YFP (C). Current families shown were evoked by 50-ms steps from -80 to -40 through 60 mV in 10-mV increments. Current amplitudes were normalized by linear cell capacitance (pA/pF). (D) I-V relationships are shown. (E) Confocal images confirming successful heterologous expression of V-Rem and V-Rem AAA in tsA201 cells are shown. Bars, 10 µm. Error bars represent ±SEM.

(see examples in Fig. S1). FDB fibers expressing V-Rem AAA produced sizable L-type currents that were not different than those observed in fibers expressing YFP (−9.8 ± 1.2 pA/pF, n = 6 and −9.0 ± 0.5 pA/pF, n = 5, respectively, at 20 mV; P > 0.05; Fig. 6 A). Likewise, V-Rem AAA had no obvious effect on the magnitude of gating charge movement (24.6 ± 3.4 nC/µF, n = 5; P > 0.05, ANOVA; Fig. 6 B and Table 1), although these fibers did present a steeper Q-V relationship when compared head-to-head with YFP-expressing fibers (P < 0.05, unpaired t test). Most importantly, V-Rem AAA also failed to significantly dampen SR Ca^{2+} release in response to membrane depolarization (1.4 ± 0.2 ΔF/F, n = 6; P > 0.05, ANOVA; Fig. 6 C and Table 1). Taken with the results in Figs. 4 and 5 showing that V-Rem AAA is unable to interact with β_{1a}, these data indicate that the near ablation of EC coupling by V-Rem (Fig. 1) is largely dependent on structural elements that are important for contact(s) with β_{1a}.

DISCUSSION

In this study, we found that the RGK family small G protein Rem profoundly inhibits skeletal muscle EC coupling in adult mouse FDB muscle fibers (Fig. 1, D–F). Because the observed reduction in voltage-induced SR Ca^{2+} release was not likely a consequence of altered $Ca_V1.1$ targeting (Fig. 3), impaired voltage sensing (Fig. 1, A–C) or a greatly depleted SR Ca^{2+} store (Fig. 2), a "communication breakdown" must have occurred between $Ca_V1.1$ and RYR1. An intuitive candidate locus for such EC uncoupling is the auxiliary β_{1a} subunit of the $Ca_V1.1$ heteromultimer because RGK proteins are established β-subunit–interacting partners (Béguin et al., 2001, 2007; Finlin et al., 2003, 2006; Yang and Colecraft, 2013; Puhl et al., 2014; Xu et al., 2015). Earlier work by Colecraft and colleagues has established that Rem can inhibit L-type $Ca_V1.2$ channels expressed in HEK 293 cells without affecting intramembrane charge movement (Yang et al., 2007, 2010), and that this particular mode

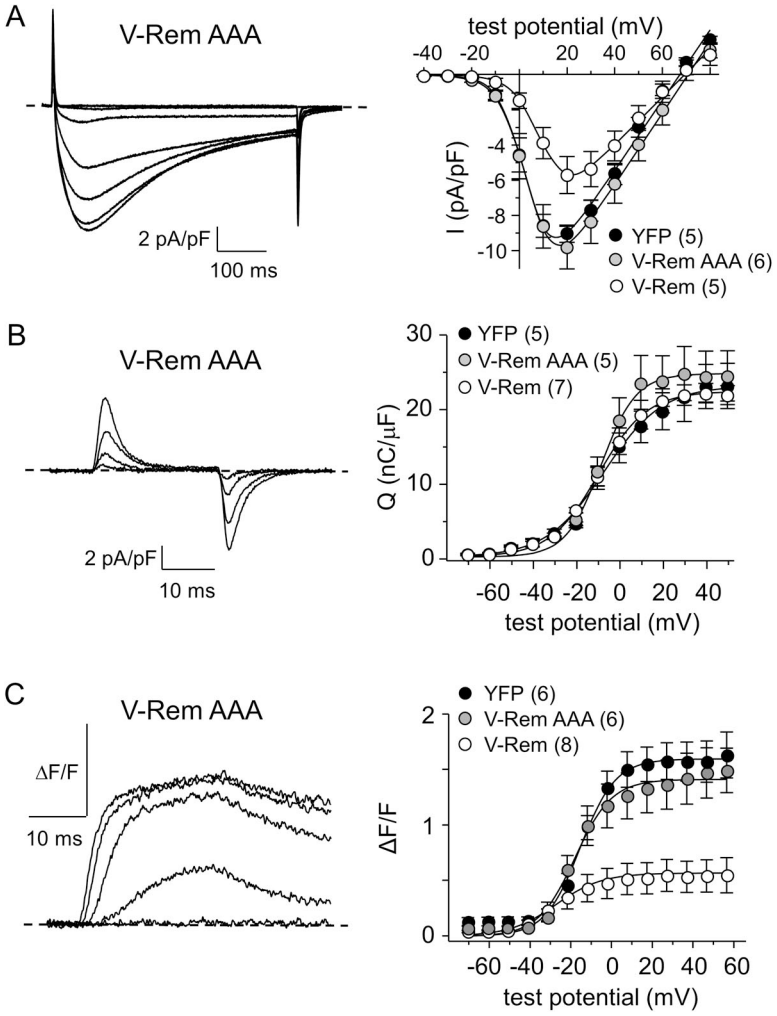

Figure 6. Expression of V-Rem AAA in FDB fibers has very little effect on native $Ca_V1.1$ function. Representative recordings of skeletal muscle L-type Ca^{2+} currents elicited by 500-ms depolarizations from −50 to −20, 0, 20, and 40 mV are shown for FDB fibers expressing V-Rem AAA (A; left). The peak I-V relationship for fibers expressing V-Rem AAA (n = 6; gray circles) is shown with the peak I-V relationship for fibers expressing unfused YFP (n = 5; black circles) and V-Rem (n = 5; white circles) in the right panel. L-type currents were evoked at 0.1 Hz by test potentials ranging from −40 through 80 mV in 10-mV increments. The smooth curves are plotted according to Eq. 2 with the following respective parameters for V-Rem AAA–, V-Rem–, and YFP-expressing fibers: G_{max} = 212 ± 26, 128 ± 19, and 205 ± 12 nS/nF; $V_{1/2}$ = 4.3 ± 3.1, 8.3 ± 3.2, and 4.0 ± 2.0 mV; k_G = 5.0 ± 0.4, 5.4 ± 0.5, and 5.1 ± 0.5 mV; V_{rev} = 70.0 ± 1.7, 70.0 ± 3.4, and 67.0 ± 1.4 mV. Representative recordings of intramembrane charge movements elicited by 25-ms depolarizations from −80 to −40, −20, 0, and 20 mV are shown for transfected FDB fibers expressing V-Rem AAA (B; left). The Q-V relationships for fibers expressing V-Rem (n = 7; white circles), V-Rem AAA (n = 5; gray circles), or YFP (n = 5; black circles) are shown in the right panel. Charge movements were evoked at 0.1 Hz by test potentials ranging from −70 through 50 mV in 10-mV increments. The smooth curves for V-Rem–, V-Rem AAA–, or YFP-expressing fibers are plotted according to Eq. 1 with the respective fit parameters shown in Table 1. Representative recordings of myoplasmic Ca^{2+} transients elicited by 25-ms depolarizations from −80 to −40, −20, 0, 20, and 40 mV are shown for FDB fibers overexpressing V-Rem AAA (C; left). The peak ΔF/F-V relationships for V-Rem AAA (n = 6; gray circles)–, V-Rem (n = 8; white circles)–, and YFP (n = 6; black circles)-expressing fibers are presented in the right panel. Ca^{2+} transients were evoked at 0.1 Hz by test potentials ranging from −70 through 60 mV in 10-mV increments. The smooth curves for V-Rem–, V-Rem AAA–, and YFP-expressing fibers are plotted according to Eq. 3 with the respective fit parameters shown in Table 1. The Q-V and ΔF/F-V relationships for YFP- and V-Rem–expressing fibers are reproduced from Fig. 1. Error bars represent ±SEM.

of Rem-mediated inhibition is dependent solely on an interaction with the β subunit (Yang et al., 2012; Yang and Colecraft, 2013). Because Rem exclusively uses this "low P_o" gating mode to inhibit $Ca_V1.1$ channel function in differentiated muscle fibers (Beqollari et al., 2014), the observed impairment of EC coupling by Rem is almost certainly dependent on a Rem-β_{1a} interaction. The inability of V-Rem AAA, a Rem construct lacking key structural elements for β binding and channel inhibition (Figs. 4 and 5, respectively), to reduce EC coupling provides additional support for this assertion (Fig. 6).

In addition to inhibiting EC coupling, V-Rem also reduced L-type current in FDB fibers (Fig. 6 A; Beqollari et al., 2014). Because L-type Ca^{2+} entry has been found to contribute to SR Ca^{2+} store refilling in myotubes (Cherednichenko et al., 2004) and in differentiated muscle fibers (Lee et al., 2015), it is not beyond possibility that SR stores may be partially depleted in V-Rem–expressing fibers. However, the nearly equivalent responses of YFP- and V-Rem–expressing fibers to 4-C*m*C (Fig. 2) support the idea that such a mechanism is unlikely to account for the observed effect of Rem on voltage-induced SR Ca^{2+} release. Likewise, an acute contribution from L-type Ca^{2+} flux via the channel is also improbable, as the ΔF/F-V curves for YFP- and Rem AAA–expressing fibers both displayed sigmoidal dependencies on voltage, a hallmark indication of skeletal-type EC coupling (see Fig. 6 C, right). If Ca^{2+} flux were making a small contribution to the transients, its loss could not likely explain the nearly 65% decrease in SR Ca^{2+} release resulting from coexpression of V-Rem.

Strong circumstantial, but by no means definitive, evidence exists supporting the hypothesis that β_{1a} is directly involved in $Ca_V1.1$–RYR1 communication (see Rebbeck et al., 2014). In particular, expression of β_{1a} is essential for EC coupling and enhances L-type current amplitude considerably (Gregg et al., 1996; Strube et al., 1996). Unfortunately, these early results obtained with myotubes cultured from β_1 null mice have been difficult to interpret because membrane expression of the principal α_{1S} subunit of $Ca_V1.1$ was severely compromised. The confounding obstacle of poor α_{1S} trafficking in β_1 null mice was overcome by elegant work with the effectively β_1 null *relaxed* zebrafish mutant line. In the *relaxed* system, unpartnered α_{1S} subunits trafficked somewhat more effectively to plasma membrane–SR junctions than in mice (Schredelseker et al., 2005). The improved membrane expression of $Ca_V1.1$ enabled meticulous ultrastructural examination of *relaxed* junctions, revealing that β_{1a} is required to organize $Ca_V1.1$ into the tetrad arrays that are prerequisite for EC coupling.

Beyond ultrastructure, the zebrafish model system poses nearly the same challenges to deciphering the function of β_{1a} as does the β_1 null mouse model. Specifically, the introduction of chimeric β_{1a} constructs or other $Ca_V\beta$ isoforms has been highly useful in the identification of functionally important domains, but information regarding essential intermolecular interactions remains frustratingly difficult to glean (Beam and Bannister, 2010). In efforts to avoid such ambiguity, in vitro approaches have been used to identify interactions of potential functional significance between β_{1a} and RYR1. Indeed, purified full-length β_{1a} subunits do bind fragments of RYR1 in vitro (Cheng et al., 2005; Rebbeck et al., 2011), and a peptide corresponding to β_{1a} residues V490–M524 increases RYR1 P_o when applied to lipid layers (Karunasekara et al., 2012). Likewise, dialysis of FDB fibers with a slightly shorter peptide (V490–M508)

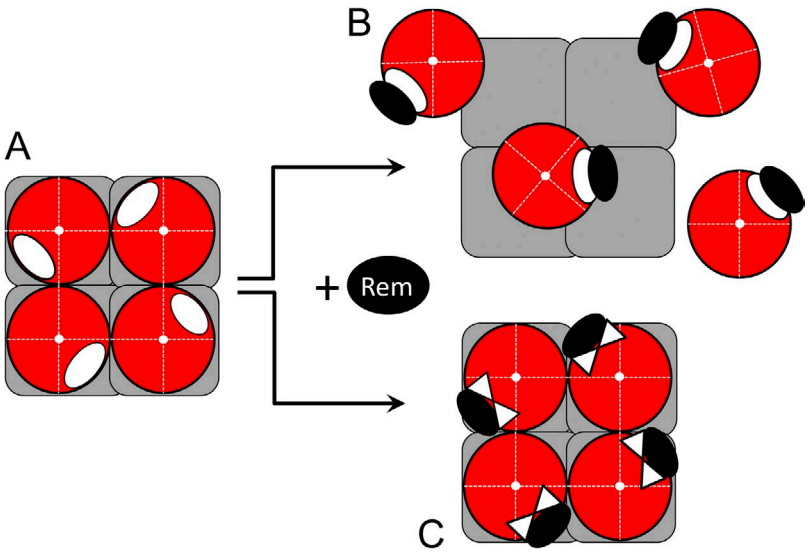

Figure 7. Schematic depicting potential mechanisms for Rem-mediated EC uncoupling. (A) The diagram represents the intact $Ca_V1.1$–RYR1 ultrastructure requisite for skeletal-type EC coupling. Four $Ca_V1.1$ α_{1S} (red circles)–β_{1a} (white ovals) channel complexes are shown coupled to each subunit of a single RYR1 (gray tetramer) from a transverse-tubular vantage point. For clarity, the β_{1a} subunits are superimposed on the α_{1S} subunits, and the $\alpha_2\delta$-1 subunits, γ_1 subunits, and other nonessential components of the junction have been omitted. The orientation of β_{1a} within the tetrad follows on previous work (Leuranguer et al., 2006; Sheridan et al., 2012). In the right panels (B and C), we present two potential mechanisms by which Rem (black ovals) may disrupt EC coupling. In B, Rem displaces the $Ca_V1.1$ channel complex from RYR1 sufficiently to disrupt the tetradic ultrastructure that is required for $Ca_V1.1$–RYR1 communication by interacting with the conserved guanylate kinase–like domain of β_{1a} (Finlin et al., 2006; Béguin et al., 2007) on the periphery of the tetrad (Szpyt et al., 2012). If ultrastructure is preserved in Rem-overexpressing fibers (as depicted in C), the binding of Rem to β_{1a} within the intact CRU would most likely induce conformational rearrangements within β_{1a} that deter transmission of the EC coupling signal from the membrane-bound, voltage-sensing regions of $Ca_V1.1$ to RYR1.

peptide potentiates both EC coupling and L-type Ca^{2+} current by nearly 50% (Hernández-Ochoa et al., 2014). Although the use of β_{1a}-based peptide approaches has provided support for the idea that β_{1a} residues V490–M508 are involved in transmitting the signal between $Ca_V1.1$ and RYR1, the interpretation of these results has been somewhat limited because of uncertainty of substrate and lack of peptide specificity; one must take into account that a variety of small peptides binds to the ginormous ∼2.3-MDa RYR1 tetramer and/or modulates RYR1 P_o in lipid bilayers (e.g., peptides corresponding to the A domain of the $Ca_V1.1$ II–III linker, Imperatoxin A, Maurocalcine; El-Hayek and Ikemoto, 1998; Gurrola et al., 1999; Fajloun et al., 2000; Nabhani et al., 2002; Chen et al., 2003; Cui et al., 2009).

In light of the frustrating limitations of the experimental approaches described above, new strategies are needed to further investigate the role of β_{1a} in skeletal-type EC coupling. The use of wild-type Rem or modified Rem constructs to probe junctional architecture represents such an advance because the small G protein disrupts $Ca_V1.1$–RYR1 communication in intact, differentiated muscle fibers without deleting or altering the peptide sequences of the endogenous components of the Ca^{2+} release unit (CRU). Obviously, the next step in this line of investigation is to determine the precise mechanism by which Rem cuts communication between $Ca_V1.1$ and RYR1. Based on what is currently known, β_{1a} coordinates the juxtaposition of $Ca_V1.1$ with RYR1 in tetrads (Fig. 7 A). So, it is quite possible that the Rem–β_{1a} interaction merely impairs the ability of β_{1a} to facilitate the ultrastructural configuration of $Ca_V1.1$ and RYR1 that is requisite for conformational coupling (Fig. 7 B). However, the preservation of tetrad arrays in fibers overexpressing Rem would indicate that the RGK protein is exerting its inhibitory influence on β_{1a} within the intact CRU, which in turn would imply that conformational changes in β_{1a} are involved in $Ca_V1.1$–RYR1 coupling (Fig. 7 C). A correlate of the latter interpretation would be that other structures (e.g., II–III loop of the α_{1S} subunit) thought to be involved in transmission of the EC coupling signal are adversely impacted by Rem-induced conformational changes in β_{1a}. Of course, these ideas remain to be tested. In this regard, our current observations provide a new means for the investigation of the β_{1a} subunit as mediator of the communication between $Ca_V1.1$ and RYR1 that underlies EC coupling skeletal muscle.

We thank Mr. M.P. Scheele for technical assistance, Drs. S.R. Ikeda and H.L. Puhl, III, for sharing the Venus-Rem expression plasmid, and Drs. K.G. Beam and D. Oskar for continued support.

This work was supported by grants from the National Institutes of Health (AG038778 to R.A. Bannister), the Colorado Clinical and Translational Sciences Institute (J-11-122 to R.A. Bannister), the Boettcher Foundation (to R.A. Bannister), and CONACyT (169006 to U. Meza). D. Beqollari received a stipend from 2T32AG000279-11 (to R.S. Schwartz, University of Colorado Denver-AMC Department of Medicine-Geriatrics Division). Confocal images were acquired in the University of Colorado Denver-AMC Advanced Light Microscopy Core (funded in part by National Institutes of Health/NCRR Colorado CTSI grant UL1 RR025780).

The authors declare no competing financial interests.

Author contributions: D. Beqollari and R.A. Bannister designed research, performed research, analyzed data, and wrote the paper. C.F. Romberg and D. Filipova performed experiments and analyzed data. U. Meza and S. Papadopoulos analyzed data and wrote the paper.

Richard L. Moss served as editor.

Submitted: 30 October 2014
Accepted: 18 May 2015

REFERENCES

Bannister, R.A., and K.G. Beam. 2013. $Ca_V1.1$: The atypical prototypical voltage-gated Ca^{2+} channel. *Biochim. Biophys. Acta.* 1828:1587–1597. http://dx.doi.org/10.1016/j.bbamem.2012.09.007

Bannister, R.A., H.M. Colecraft, and K.G. Beam. 2008. Rem inhibits skeletal muscle EC coupling by reducing the number of functional L-type Ca^{2+} channels. *Biophys. J.* 94:2631–2638. http://dx.doi.org/10.1529/biophysj.107.116467

Beam, K.G., and R.A. Bannister. 2010. Perspectives on: SGP Symposium on Muscle in Health and Disease: Looking for answers to EC coupling's persistent questions. *J. Gen. Physiol.* 136:7–12. http://dx.doi.org/10.1085/jgp.201010461

Béguin, P., K. Nagashima, T. Gonoi, T. Shibasaki, K. Takahashi, Y. Kashima, N. Ozaki, K. Geering, T. Iwanaga, and S. Seino. 2001. Regulation of Ca^{2+} channel expression at the cell surface by the small G-protein kir/Gem. *Nature.* 411:701–706. http://dx.doi.org/10.1038/35079621

Béguin, P., Y.J. Ng, C. Krause, R.N. Mahalakshmi, M.Y. Ng, and W. Hunziker. 2007. RGK small GTP-binding proteins interact with the nucleotide kinase domain of Ca^{2+}-channel β-subunits via an uncommon effector binding domain. *J. Biol. Chem.* 282:11509–11520. http://dx.doi.org/10.1074/jbc.M606423200

Beqollari, D., C.F. Romberg, U. Meza, S. Papadopoulos, and R.A. Bannister. 2014. Differential effects of RGK proteins on L-type channel function in adult mouse skeletal muscle. *Biophys. J.* 106:1950–1957. http://dx.doi.org/10.1016/j.bpj.2014.03.033

Beqollari, D., C.F. Romberg, D. Filipova, S. Papadopoulos, and R.A. Bannister. 2015. Functional assessment of three Rem residues identified as critical for interactions with Ca^{2+} channel β subunits. *Pflugers Arch.* In press.

Chen, L., E. Estève, J.M. Sabatier, M. Ronjat, M. De Waard, P.D. Allen, and I.N. Pessah. 2003. Maurocalcine and peptide A stabilize distinct subconductance states of ryanodine receptor type 1, revealing a proportional gating mechanism. *J. Biol. Chem.* 278:16095–16106. http://dx.doi.org/10.1074/jbc.M209501200

Cheng, W., X. Altafaj, M. Ronjat, and R. Coronado. 2005. Interaction between the dihydropyridine receptor Ca^{2+} channel β-subunit and ryanodine receptor type 1 strengthens excitation-contraction coupling. *Proc. Natl. Acad. Sci. USA.* 102:19225–19230. http://dx.doi.org/10.1073/pnas.0504334102

Cherednichenko, G., A.M. Hurne, J.D. Fessenden, E.H. Lee, P.D. Allen, K.G. Beam, and I.N. Pessah. 2004. Conformational activation of Ca^{2+} entry by depolarization of skeletal myotubes. *Proc. Natl. Acad. Sci. USA.* 101:15793–15798. http://dx.doi.org/10.1073/pnas.0403485101

Cui, Y., H.S. Tae, N.C. Norris, Y. Karunasekara, P. Pouliquin, P.G. Board, A.F. Dulhunty, and M.G. Casarotto. 2009. A dihydropyridine receptor α_{1s} loop region critical for skeletal muscle contraction is intrinsically unstructured and binds to a SPRY domain of

the type 1 ryanodine receptor. *Int. J. Biochem. Cell Biol.* 41:677–686. http://dx.doi.org/10.1016/j.biocel.2008.08.004

Dayal, A., J. Schredelseker, C. Franzini-Armstrong, and M. Grabner. 2010. Skeletal muscle excitation-contraction coupling is independent of a conserved heptad repeat motif in the C-terminus of the DHPR β_{1a} subunit. *Cell Calcium.* 47:500–506. http://dx.doi.org/10.1016/j.ceca.2010.04.003

Dayal, A., V. Bhat, C. Franzini-Armstrong, and M. Grabner. 2013. Domain cooperativity in the β_{1a} subunit is essential for dihydropyridine receptor voltage sensing in skeletal muscle. *Proc. Natl. Acad. Sci. USA.* 110:7488–7493. http://dx.doi.org/10.1073/pnas.1301087110

DiFranco, M., J. Capote, M. Quiñonez, and J.L. Vergara. 2007. Voltage-dependent dynamic FRET signals from the transverse tubules in mammalian skeletal muscle fibers. *J. Gen. Physiol.* 130: 581–600. http://dx.doi.org/10.1085/jgp.200709831

DiFranco, M., P. Tran, M. Quiñonez, and J.L. Vergara. 2011. Functional expression of transgenic α1sDHPR channels in adult mammalian skeletal muscle fibres. *J. Physiol.* 589:1421–1442. http://dx.doi.org/10.1113/jphysiol.2010.202804

El-Hayek, R., and N. Ikemoto. 1998. Identification of the minimum essential region in the II-III loop of the dihydropyridine receptor α_1 subunit required for activation of skeletal muscle-type excitation-contraction coupling. *Biochemistry.* 37:7015–7020. http://dx.doi.org/10.1021/bi972907o

Eltit, J.M., C. Franzini-Armstrong, and C.F. Perez. 2014. Amino acid residues 489-503 of dihydropyridine receptor (DHPR) β_{1a} subunit are critical for structural communication between the skeletal muscle DHPR complex and type 1 ryanodine receptor. *J. Biol. Chem.* 289:36116–36124. http://dx.doi.org/10.1074/jbc.M114.615526

Fajloun, Z., R. Kharrat, L. Chen, C. Lecomte, E. Di Luccio, D. Bichet, M. El Ayeb, H. Rochat, P.D. Allen, I.N. Pessah, et al. 2000. Chemical synthesis and characterization of maurocalcine, a scorpion toxin that activates Ca^{2+} release channel/ryanodine receptors. *FEBS Lett.* 469:179–185. http://dx.doi.org/10.1016/S0014-5793(00)01239-4

Finlin, B.S., S.M. Crump, J. Satin, and D.A. Andres. 2003. Regulation of voltage-gated calcium channel activity by the Rem and Rad GTPases. *Proc. Natl. Acad. Sci. USA.* 100:14469–14474. http://dx.doi.org/10.1073/pnas.2437756100

Finlin, B.S., R.N. Correll, C. Pang, S.M. Crump, J. Satin, and D.A. Andres. 2006. Analysis of the complex between Ca^{2+} channel β-subunit and the Rem GTPase. *J. Biol. Chem.* 281:23557–23566. http://dx.doi.org/10.1074/jbc.M604867200

Flynn, R., and G.W. Zamponi. 2010. Regulation of calcium channels by RGK proteins. *Channels (Austin).* 4:434–439. http://dx.doi.org/10.4161/chan.4.6.12865

García, J., T. Tanabe, and K.G. Beam. 1994. Relationship of calcium transients to calcium currents and charge movements in myotubes expressing skeletal and cardiac dihydropyridine receptors. *J. Gen. Physiol.* 103:125–147. http://dx.doi.org/10.1085/jgp.103.1.125

Gregg, R.G., A. Messing, C. Strube, M. Beurg, R. Moss, M. Behan, M. Sukhareva, S. Haynes, J.A. Powell, R. Coronado, and P.A. Powers. 1996. Absence of the β subunit (*cchb1*) of the skeletal muscle dihydropyridine receptor alters expression of the α_1 subunit and eliminates excitation-contraction coupling. *Proc. Natl. Acad. Sci. USA.* 93:13961–13966. http://dx.doi.org/10.1073/pnas.93.24.13961

Gurrola, G.B., C. Arévalo, R. Sreekumar, A.J. Lokuta, J.W. Walker, and H.H. Valdivia. 1999. Activation of ryanodine receptors by imperatoxin A and a peptide segment of the II-III loop of the dihydropyridine receptor. *J. Biol. Chem.* 274:7879–7886. http://dx.doi.org/10.1074/jbc.274.12.7879

Hernández-Ochoa, E.O., R.O. Olojo, R.T. Rebbeck, A.F. Dulhunty, and M.F. Schneider. 2014. β_{1a}490-508, a 19-residue peptide from C-terminal tail of $Ca_v1.1$ β_{1a} subunit, potentiates voltage-dependent calcium release in adult skeletal muscle fibers. *Biophys. J.* 106:535–547. http://dx.doi.org/10.1016/j.bpj.2013.11.4503

Jhun, B.S., J. O-Uchi, W. Wang, C.H. Ha, J. Zhao, J.Y. Kim, C. Wong, R.T. Dirksen, C.M. Lopes, and Z.G. Jin. 2012. Adrenergic signaling controls RGK-dependent trafficking of cardiac voltage-gated L-type Ca^{2+} channels through PKD1. *Circ. Res.* 110:59–70. http://dx.doi.org/10.1161/CIRCRESAHA.111.254672

Karunasekara, Y., R.T. Rebbeck, L.M. Weaver, P.G. Board, A.F. Dulhunty, and M.G. Casarotto. 2012. An α-helical C-terminal tail segment of the skeletal L-type Ca^{2+} channel β_{1a} subunit activates ryanodine receptor type 1 via a hydrophobic surface. *FASEB J.* 26:5049–5059. http://dx.doi.org/10.1096/fj.12-211334

Lee, C.S., A. Dagnino-Acosta, V. Yarotskyy, A. Hanna, A. Lyfenko, M. Knoblauch, D.K. Georgiou, R.A. Poché, M.W. Swank, C. Long, et al. 2015. Ca^{2+} permeation and/or binding to $Ca_V1.1$ fine-tunes skeletal muscle Ca^{2+} signaling to sustain muscle function. *Skelet. Muscle.* 5:4.

Leuranguer, V., S. Papadopoulos, and K.G. Beam. 2006. Organization of calcium channel β_{1a} subunits in triad junctions in skeletal muscle. *J. Biol. Chem.* 281:3521–3527. http://dx.doi.org/10.1074/jbc.M509566200

Lu, X., L. Xu, and G. Meissner. 1994. Activation of the skeletal muscle calcium release channel by a cytoplasmic loop of the dihydropyridine receptor. *J. Biol. Chem.* 269:6511–6516.

Mahalakshmi, R.N., M.Y. Ng, K. Guo, Z. Qi, W. Hunziker, and P. Béguin. 2007. Nuclear localization of endogenous RGK proteins and modulation of cell shape remodeling by regulated nuclear transport. *Traffic.* 8:1164–1178. http://dx.doi.org/10.1111/j.1600-0854.2007.00599.x

Meza, U., D. Beqollari, C.F. Romberg, S. Papadopoulos, and R.A. Bannister. 2013. Potent inhibition of L-type Ca^{2+} currents by a Rad variant associated with congestive heart failure. *Biochem. Biophys. Res. Commun.* 439:270–274. http://dx.doi.org/10.1016/j.bbrc.2013.08.044

Murata, M., E. Cingolani, A.D. McDonald, J.K. Donahue, and E. Marbán. 2004. Creation of a genetic calcium channel blocker by targeted gem gene transfer in the heart. *Circ. Res.* 95:398–405. http://dx.doi.org/10.1161/01.RES.0000138449.85324.c5

Nabhani, T., X. Zhu, I. Simeoni, V. Sorrentino, H.H. Valdivia, and J. García. 2002. Imperatoxin A enhances Ca^{2+} release in developing skeletal muscle containing ryanodine receptor type 3. *Biophys. J.* 82:1319–1328. http://dx.doi.org/10.1016/S0006-3495(02)75487-8

Nakai, J., R.T. Dirksen, H.T. Nguyen, I.N. Pessah, K.G. Beam, and P.D. Allen. 1996. Enhanced dihydropyridine receptor channel activity in the presence of ryanodine receptor. *Nature.* 380:72–75. http://dx.doi.org/10.1038/380072a0

Nakai, J., T. Tanabe, T. Konno, B. Adams, and K.G. Beam. 1998. Localization in the II-III loop of the dihydropyridine receptor of a sequence critical for excitation-contraction coupling. *J. Biol. Chem.* 273:24983–24986. http://dx.doi.org/10.1074/jbc.273.39.24983

Ono, F., G. Mandel, and P. Brehm. 2004. Acetylcholine receptors direct rapsyn clusters to the neuromuscular synapse in zebrafish. *J. Neurosci.* 24:5475–5481. http://dx.doi.org/10.1523/JNEUROSCI.0851-04.2004

Papadopoulos, S., V. Leuranguer, R.A. Bannister, and K.G. Beam. 2004. Mapping sites of potential proximity between the dihydropyridine receptor and RyR1 in muscle using a cyan fluorescent protein-yellow fluorescent protein tandem as a fluorescence resonance energy transfer probe. *J. Biol. Chem.* 279:44046–44056. http://dx.doi.org/10.1074/jbc.M405317200

Prosser, B.L., E.O. Hernández-Ochoa, D.B. Zimmer, and M.F. Schneider. 2009. The Q_γ component of intra-membrane charge

movement is present in mammalian muscle fibres, but suppressed in the absence of S100A1. *J. Physiol.* 587:4523–4541. http://dx.doi.org/10.1113/jphysiol.2009.177238

Puhl, H.L., III, V.B. Lu, Y.-J. Won, Y. Sasson, J.A. Hirsch, F. Ono, and S.R. Ikeda. 2014. Ancient origins of RGK protein function: Modulation of voltage-gated calcium channels preceded the protostome and deuterostome split. *PLoS ONE.* 9:e100694. http://dx.doi.org/10.1371/journal.pone.0100694

Rebbeck, R.T., Y. Karunasekara, E.M. Gallant, P.G. Board, N.A. Beard, M.G. Casarotto, and A.F. Dulhunty. 2011. The β_{1a} subunit of the skeletal DHPR binds to skeletal RyR1 and activates the channel via its 35-residue C-terminal tail. *Biophys. J.* 100:922–930. http://dx.doi.org/10.1016/j.bpj.2011.01.022

Rebbeck, R.T., Y. Karunasekara, P.G. Board, N.A. Beard, M.G. Casarotto, and A.F. Dulhunty. 2014. Skeletal muscle excitation-contraction coupling: Who are the dancing partners? *Int. J. Biochem. Cell Biol.* 48:28–38. http://dx.doi.org/10.1016/j.biocel.2013.12.001

Ríos, E., and G. Brum. 1987. Involvement of dihydropyridine receptors in excitation-contraction coupling in skeletal muscle. *Nature.* 325:717–720. http://dx.doi.org/10.1038/325717a0

Romberg, C.F., D. Beqollari, U. Meza, and R.A. Bannister. 2014. RGK protein-mediated impairment of slow depolarization-dependent Ca^{2+} entry into developing myotubes. *Channels (Austin).* 8:243–248. http://dx.doi.org/10.4161/chan.27686

Schneider, M.F., and W.K. Chandler. 1973. Voltage dependent charge movement of skeletal muscle: a possible step in excitation-contraction coupling. *Nature.* 242:244–246. http://dx.doi.org/10.1038/242244a0

Schredelseker, J., V. Di Biase, G.J. Obermair, E.T. Felder, B.E. Flucher, C. Franzini-Armstrong, and M. Grabner. 2005. The β_{1a} subunit is essential for the assembly of dihydropyridine-receptor arrays in skeletal muscle. *Proc. Natl. Acad. Sci. USA.* 102:17219–17224. http://dx.doi.org/10.1073/pnas.0508710102

Schredelseker, J., A. Dayal, T. Schwerte, C. Franzini-Armstrong, and M. Grabner. 2009. Proper restoration of excitation-contraction coupling in the dihydropyridine receptor β_1-null zebrafish *relaxed* is an exclusive function of the β_{1a} subunit. *J. Biol. Chem.* 284:1242–1251. http://dx.doi.org/10.1074/jbc.M807767200

Sheridan, D.C., O. Moua, N.M. Lorenzon, and K.G. Beam. 2012. Bimolecular fluorescence complementation and targeted biotinylation provide insight into the topology of the skeletal muscle Ca^{2+} channel β_{1a} subunit. *Channels (Austin).* 6:26–40. http://dx.doi.org/10.4161/chan.18916

Strube, C., M. Beurg, P.A. Powers, R.G. Gregg, and R. Coronado. 1996. Reduced Ca^{2+} current, charge movement, and absence of Ca^{2+} transients in skeletal muscle deficient in dihydropyridine receptor β_1 subunit. *Biophys. J.* 71:2531–2543. http://dx.doi.org/10.1016/S0006-3495(96)79446-8

Szpyt, J., N. Lorenzon, C.F. Perez, E. Norris, P.D. Allen, K.G. Beam, and M. Samsó. 2012. Three-dimensional localization of the α and β subunits and of the II-III loop in the skeletal muscle L-type Ca^{2+} channel. *J. Biol. Chem.* 287:43853–43861. http://dx.doi.org/10.1074/jbc.M112.419283

Tanabe, T., K.G. Beam, J.A. Powell, and S. Numa. 1988. Restoration of excitation-contraction coupling and slow calcium current in dysgenic muscle by dihydropyridine receptor complementary DNA. *Nature.* 336:134–139. http://dx.doi.org/10.1038/336134a0

Tanabe, T., K.G. Beam, B.A. Adams, T. Niidome, and S. Numa. 1990. Regions of the skeletal muscle dihydropyridine receptor critical for excitation-contraction coupling. *Nature.* 346:567–569. http://dx.doi.org/10.1038/346567a0

Wang, Z.M., M.L. Messi, and O. Delbono. 1999. Patch-clamp recording of charge movement, Ca^{2+} current, and Ca^{2+} transients in adult skeletal muscle fibers. *Biophys. J.* 77:2709–2716. http://dx.doi.org/10.1016/S0006-3495(99)77104-3

Wilkens, C.M., N. Kasielke, B.E. Flucher, K.G. Beam, and M. Grabner. 2001. Excitation-contraction coupling is unaffected by drastic alteration of the sequence surrounding residues L720-L764 of the α_{1S} II-III loop. *Proc. Natl. Acad. Sci. USA.* 98:5892–5897. http://dx.doi.org/10.1073/pnas.101618098

Wu, F., W. Mi, E.O. Hernández-Ochoa, D.K. Burns, Y. Fu, H.F. Gray, A.F. Struyk, M.F. Schneider, and S.C. Cannon. 2012. A calcium channel mutant mouse model of hypokalemic periodic paralysis. *J. Clin. Invest.* 122:4580–4591. http://dx.doi.org/10.1172/JCI66091

Xu, X., F. Zhang, G.W. Zamponi, and W.A. Horne. 2015. Solution NMR and calorimetric analysis of Rem2 binding to the Ca^{2+} channel β_4 subunit: a low affinity interaction is required for inhibition of $Ca_V2.1$ Ca^{2+} currents. *FASEB J.* 29:1794–1804. http://dx.doi.org/10.1096/fj.14-264499

Yang, T., and H.M. Colecraft. 2013. Regulation of voltage-dependent calcium channels by RGK proteins. *Biochim. Biophys. Acta.* 1828:1644–1654. http://dx.doi.org/10.1016/j.bbamem.2012.10.005

Yang, T., Y. Suhail, S. Dalton, T. Kernan, and H.M. Colecraft. 2007. Genetically encoded molecules for inducibly inactivating Ca_V channels. *Nat. Chem. Biol.* 3:795–804. http://dx.doi.org/10.1038/nchembio.2007.42

Yang, T., X. Xu, T. Kernan, V. Wu, and H.M. Colecraft. 2010. Rem, a member of the RGK GTPases, inhibits recombinant $Ca_V1.2$ channels using multiple mechanisms that require distinct conformations of the GTPase. *J. Physiol.* 588:1665–1681. http://dx.doi.org/10.1113/jphysiol.2010.187203

Yang, T., A. Puckerin, and H.M. Colecraft. 2012. Distinct RGK GTPases differentially use α_1- and auxiliary β-binding-dependent mechanisms to inhibit $Ca_V1.2/Ca_V2.2$ channels. *PLoS ONE.* 7: e37079. http://dx.doi.org/10.1371/journal.pone.0037079